Smart Structures and Systems, Vol. 7, No. 1 (2011) 59-82
DOI: http://dx.doi.org/10.12989/sss.2011.7.1.059

Output-only modal identification approach for time-unsynchronized signals from decentralized wireless sensor network for linear structural systems

Jae-Hyung Park[1a], Jeong-Tae Kim*[2b] and Jin-Hak Yi[3c]

[1]*Department of Ocean Engineering, Pukyong National University, Busan, Korea*
[2]*Department of Ocean Engineering, Pukyong National University, Busan 608-737, Korea*
[3]*Korea Ocean Research & Development Institute, Ansan, Korea*

(Received September 2, 2010, Accepted December 9, 2010)

Abstract. In this study, an output-only modal identification approach is proposed for decentralized wireless sensor nodes used for linear structural systems. The following approaches are implemented to achieve the objective. Firstly, an output-only modal identification method is selected for decentralized wireless sensor networks. Secondly, the effect of time-unsynchronization is assessed with respect to the accuracy of modal identification analysis. Time-unsynchronized signals are analytically examined to quantify uncertainties and their corresponding errors in modal identification results. Thirdly, a modified approach using complex mode shapes is proposed to reduce the unsynchronization-induced errors in modal identification. In the new way, complex mode shapes are extracted from unsynchronized signals to deal both with modal amplitudes and with phase angles. Finally, the feasibility of the proposed approach is evaluated from numerical and experimental tests by comparing with the performance of existing approach using real mode shapes.

Keywords: output-only modal identification; wireless sensor network; time-delayed signals; time-unsynchronization effect; complex mode shapes.

1. Introduction

Structural health monitoring (SHM) systems are widely adopted to monitor the structural responses, to detect damage, and to assess the effect of damage on the structural integrity. Many researchers have developed novel sensing technologies and damage monitoring techniques for the vibration-based SHM applications (Doebling *et al.* 1998, Farrar 2001, Kim *et al.* 2003, Lee and Yun 2006, Nagayama 2007, Park 2009, Park and Kim 2009). Recently, many long-span bridges have the SHM systems installed during their constructions. Tsing Ma Suspension Bridge in Hong Kong and Seohae Grand Bridge in Korea are two good examples among many others around the world.

The SHM system is consisted of many sensors, signal transmitting wires, data acquisition (DAQ) instruments, and a centralized data storage server. Once data are stored by wired transmission into

*Corresponding Author, Professor, E-mail: idis@pknu.ac.kr
[a]Postdoctoral Researcher
[b]Professor
[c]Principal Research Scientist

the centralized servers, the off-line signals are processed for information analysis, damage monitoring, and safety evaluation. However, the costs associated with installation and maintenance of the wired SHM systems can be very high. For example, the Tsing Ma Suspension Bridge in Hong Kong was instrumented with over 350 sensors and a wired-based monitoring system which costs over 8 million US dollars (Farrar 2001). Furthermore, the cost and time for installation of the wired SHM system are inefficient since the installation cost is up to 25% of total system cost and the installation time can be over 75% of the total installation time (Straser and Kiremidjian 1998).

The high cost associated with the wired SHM system can be greatly reduced by adopting wireless sensor networks (Lynch *et al.* 2006). One of great advantages for using wireless sensors is that autonomous operations can be implemented for SHM by embedding advanced system technologies into wireless sensor nodes. Therefore, the new paradigm by adopting wireless sensor nodes may offer, but not limited, automated and cost-efficient SHM (Lynch *et al.* 2003, Nagayama *et al.* 2007, Weng *et al.* 2008, Park *et al.* 2010). However, there also exist several problems that should be solved in order to realize the SHM using wireless sensor nodes. Those issues include time-synchronization among smart sensor nodes, limited memory and battery power, and embedded algorithms for damage detection (Straser and Kiremidjian 1998, Lynch *et al.* 2003, Spencer *et al.* 2004, Kurata *et al.* 2005, Nagayama *et al.* 2007, Krishnamurthy *et al.* 2008, Lu *et al.* 2008, Nagayama *et al.* 2009, Park *et al*. 2008, 2010, Park 2009).

Among those, many researchers have noticed the importance of time-synchronization in wireless sensor networks (Nagayama 2007, Weng *et al.* 2008, Krishnamurthy *et al.* 2008). Nagayama (2007) verified mathematically that the error of time-synchronization affects mode-shapes estimated by the NExT/ERA (Natural Excitation Technique/Eigensystem Realization Algorithm) method. He proposed a resample-based algorithm using curve-fitting and low-pass filters to minimize the error due to time-unsynchronization effects. Krishnamurthy *et al.* (2008) evaluated the effect of time-synchronization on the frequency domain decomposition method by using numerical and experimental tests. They developed techniques of avoiding time-unsynchronization effects by matching local clocks. However, their modal identification approaches were rather oriented to wired systems but not wireless systems.

In this study, an output-only modal identification approach is proposed for decentralized wireless sensor nodes used for linear structural systems. The following approaches are implemented to achieve the objective. Firstly, an output-only modal identification method is selected for decentralized wireless sensor networks. Secondly, the effect of time-unsynchronization is assessed with respect to the accuracy of modal identification. Time-unsynchronized signals are analytically examined to quantify uncertainties and their corresponding errors in modal identification results. Thirdly, a modified approach using complex mode shapes is proposed to reduce the unsynchronization-induced errors in modal identification. In the new way, complex mode shapes are extracted from unsynchronized signals to deal both with modal amplitudes and with phase angles. Finally, the feasibility of the proposed approach is evaluated from numerical and experimental tests by comparing with an existing approach using real mode shapes.

2. Output-only modal identification methods for wireless sensor networks

To date, many output-only modal identification methods have been developed. They can be classified into frequency domain and time domain methods. As the frequency domain methods, peak-peaking (PP) method (Bendat and Piersol 1993) and frequency domain decomposition (FDD) method (Brinker

et al. 2001) are broadly used for experimental modal analysis. The time domain methods include Ibrahim time domain (ITD) method (Ibrahim and Mikulcik 1977), eigensystem realization algorithm (ERA) method (Juang and Pappa 1985), stochastic subspace identification and balanced realization (SSI/BR) method (Overschee and De Moor 1996), and SSI and canonical variate analysis (SSI/CVA) method (Hermans and Van Der Auweraer 1999).

Yi (2001) and Yi and Yun (2004) evaluated the performances of the output-only modal identification methods by numerical and experimental tests. Based on the evaluation results, they concluded as: the ERA, SSI/BR, and SSI/CVA methods are more reliable and accurate but require larger computation time than others; and the FDD or ITD methods have the computational efficiency and the reasonable accuracy.

For implementing the output-only modal identification under wireless sensor networks, a time-domain method, ERA, was considered by Nagayama *et al.* (2009). In order to implement the ERA method into wireless sensors, as shown in Fig. 1, Nagayama *et al.* (2009) proposed a decentralized correlation function estimation scheme to overcome the shortages of the ERA method that requires

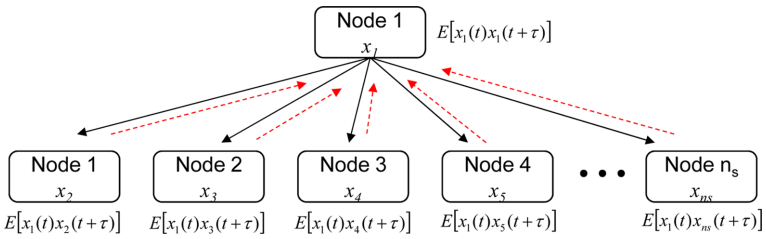

Fig. 1 Decentralized correlation function estimation for ERA (Nagayama *et al.* 2009)

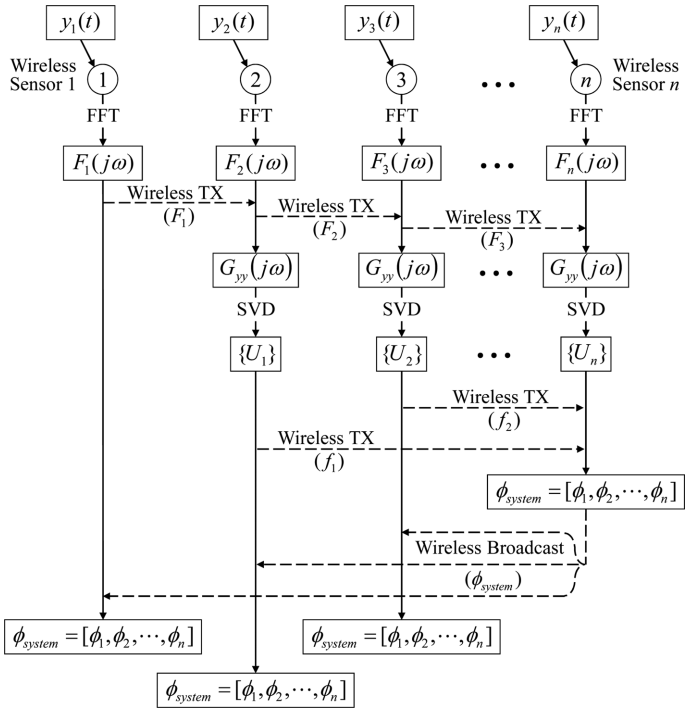

Fig. 2 Decentralized FDD method (Zimmerman *et al.* 2008)

large memory capacity, manipulation of large matrices and many data to be transmitted from wireless sensors. In that case, the total data to be transmitted are reduced to $N+N/2\times(n_s-1)$ where N is the number of data and n_s is the number of sensors while the total data in a centralized network is $N\times(n_s-1)$. That is, the total data is reduced to about 50% by using the decentralized scheme. Although the number of data is reduced, a sentry node (i.e., Node 1 in Fig. 1) still needs a large memory repository when a number of sensors are involved.

On the other side, Zimmerman *et al.* (2008) considered the FDD method which is one of frequency domain methods as shown in Fig. 2. By assuming that modal frequencies are known in prior, the total data to be transmitted can be quite reduced to $(2\times(n_s-1)+2\times(n_s-2))\times(NM)$ where NM is the number of vibration modes. Note that each sensor node transmits only real and imaginary values (i.e., 2 values) for each known frequency after fast Fourier transform (FFT) into the designed next sensor node. Assuming that the number of sensors, data and modes are 7 (n_s = 7), 1024 (N = 1024) and 4 (NM = 4), respectively, the total data is reduced to about 1.4%. The number of transmitting data can be more reduced if the reference *sentry* node can broadcast data to all other *leaf* nodes. In that case, the total data becomes to $(2+2\times(n_s-1))\times(NM)$ and is reduced to about 0.9%.

The amount of computation and the number of data to be transmitted are directly associated with the efficiency of energy depending on battery power. Based on the above considerations, in this study, the decentralized FDD method was selected to extract mode shapes under wireless sensor networks, in which the reference *sentry* node can broadcast data to all other *leaf* nodes.

3. Modal identification approach for time-unsynchronized signals

Time-synchronization is an important topic in the area of wireless sensor networks (Nagayama 2007, Krishnamurthy *et al.* 2008). In modal identification process, time-synchronization errors cause mode-shape phases and result in mode-shape errors as well as fault damage detection. In this study, a modified FDD approach using complex mode shapes is proposed to reduce the unsynchronization-induced errors in modal identification. In the new way, complex mode shapes are extracted from unsynchronized signals to deal both with modal amplitudes and with phase angles.

The FDD method estimates modal parameters (i.e., natural frequencies and mode-shapes) by utilizing the singular value decomposition (SVD) of the power spectral density (PSD) matrix. The process of FDD method is summarized as below (Brincker *et al.* 2001):

(1) To acquire a set of output responses $x_i(t)(i = 1,...,n)$ from n sensors on a structure;

(2) To construct PSD matrix as the following Eq. (1) by using cross-spectral density function $S_{km}(\omega) = E[X_k\ (\omega,\ T)X_m(\omega,\ T)]/T$, where $X_k(\omega,\ T)$ and $X_m(\omega,\ T)$ are frequency responses calculated by Fourier transforms of $x_k(t)$ and $x_m(t)$ for a constant interval T, respectively, and ω is an arbitrary frequency.

$$\mathbf{S}_{n\times n}(\omega) = \begin{bmatrix} S_{11}(\omega) & S_{12}(\omega) & \cdots & S_{1n}(\omega) \\ S_{21}(\omega) & S_{22}(\omega) & \cdots & S_{2n}(\omega) \\ \vdots & \vdots & \ddots & \vdots \\ S_{n1}(\omega) & S_{n2}(\omega) & \cdots & S_{nn}(\omega) \end{bmatrix} \tag{1}$$

where $\mathbf{S}_{n\times n}(\omega)$ is the $n\times n$ PSD matrix for output responses;

(3) To decompose the PSD matrix by using the SVD

$$\mathbf{S}_{n\times n}(\omega) = \mathbf{U}(\omega)^T\Sigma(\omega)\mathbf{V}(\omega) \tag{2}$$

where $\Sigma(\omega)$ is a $n \times n$ diagonal matrix containing the singular values of its PSD matrix, and $\mathbf{U}(\omega)$ and $\mathbf{V}(\omega)$ are $n \times n$ unitary matrices. $\mathbf{U}(\omega)$ is equal to herein $\mathbf{V}(\omega)$ since $\mathbf{S}_{n\times n}(\omega)$ is symmetric;

(4) To take the main diagonal $\sigma_i(\varpi)(i = 1,..., n)$ of $\Sigma(\varpi)$ for all frequencies ϖ;

(5) To find peak frequency $\omega_p(p = 1,...,NM)$ (i.e., natural frequency) in the first singular values $\sigma_1(\varpi)$, where ω_p denotes the p^{th} peak frequency, $\omega_p \in \varpi$ and NM is the number of modes; and

(6) To extract mode shapes from the first column vector of $\mathbf{U}(\omega_p)$ at the corresponding peak frequency ω_p.

Generally, many types of civil structures can be assumed as linear structural systems with light damping. If vibration signals of multiple locations in a linear structure are measured simultaneously, the PSD matrix and $\mathbf{U}(\omega)$ (i.e., mode shapes) are consisted of only real values. Assuming the data measured from the k^{th} sensor is delayed t_0, however, the PSD matrix for the p^{th} peak frequency ω_p is changed as follow (Krishnamurthy *et al.* 2008)

$$\mathbf{S}_{n\times n}(\omega_p) = \begin{bmatrix} \mathrm{S}_{11}(\omega_p) & \cdots & e^{-j\omega_m t_0}\mathrm{S}_{1k}(\omega_p) & \cdots & \mathrm{S}_{1n}(\omega_p) \\ \vdots & \ddots & \vdots & \cdots & \vdots \\ e^{j\omega_m t_0}\mathrm{S}_{k1}(\omega_p) & \cdots & \mathrm{S}_{kk}(\omega_p) & \cdots & e^{j\omega_m t_0}\mathrm{S}_{kn}(\omega_p) \\ \vdots & \cdots & \vdots & \ddots & \vdots \\ \mathrm{S}_{n1}(\omega_p) & \cdots & e^{-j\omega_m t_0}\mathrm{S}_{nk}(\omega_p) & \cdots & \mathrm{S}_{nn}(\omega_p) \end{bmatrix} \tag{3}$$

By the singular value decomposition of the PSD matrix, the p^{th} modal value at the k^{th} location ($\bar{\phi}_{mk}$) is obtained by

$$\bar{\phi}_{pk} = \exp(-j\omega_p t_0)\phi_{pk} \tag{4}$$

where $\bar{\phi}_{pk}$ is a complex value, j denotes $\sqrt{-1}$ and ϕ_{pk} is the p^{th} modal value without time-delay at the k^{th} location. In this case, the exact mode shape can be obtained from the magnitude of a complex value (i.e., the absolute value of $\bar{\phi}_{pk}$) as shown in Eq. (5). In addition, the time-delay t_0 can be estimated by Eq. (6).

$$\phi_{pk} = \mathrm{sign}[\cos(\theta_{pk})] \times |\bar{\phi}_{pk}| \tag{5}$$

$$t_0 = \theta_{pk}/\omega_p \tag{6}$$

where θ_{pk} is the phase angle of complex mode shape $\bar{\phi}_{pk}$. Note that $\bar{\phi}_{pk}$ and θ_{pk} are extracted by the FDD technique. The procedure to obtain exact mode shapes from time-unsynchronized signals is summarized as following two steps.

Step 1: Complex mode shapes from time-unsynchronized signals are extracted by the general FDD process as aforementioned;

Step 2: Exact modal values are calculated by using Eq. (5) for each modal values of the complex mode shapes.

In general, complex mode-shapes appear under the following circumstances (Ewins 2000, Maia and Silva 1997): 1) when measurement is poor; 2) when damping is distributed in a non-proportional way; 3) when operational deflection shapes, which is not mode-shapes, are extracted; 4) when structures contain rotating components; and 5) when two or more modes are closely spaced. Among those, the last three reasons are not necessarily considered for civil structures such as bridges. The operational deflection shapes can be identified if dynamic properties of the structure are known. The phase of mode-shape caused by rotating components is mainly extracted in mechanical systems with

turbine or aircrafts. Also, the modes of civil structures are relatively well-separated.

For the first reason, the complex mode shape is mainly occurred by the changed phase angle shifted due to experimental noise and it becomes worse in phase-angle shift when the systematic error is caused by time-unsynchronization (Park 2009). The second reason is usually associated with structural joint and structural damage. In general, mode-shapes are approximately extracted from real values of complex mode-shapes (hereafter, *real* mode-shape) by assuming that damping is changed relatively small at the structural joint and damaged location. To use magnitudes of complex mode-shapes (hereafter, *complex* mode-shape) as shown in Eq. (5), therefore, the effect for noise and damage on modal identification should be investigated in detail.

4. Evaluation of time-unsynchronization effect on modal identification approach

In order to evaluate the effect of time-unsynchronization on the proposed modal identification approach, numerical and experimental tests are performed. For the numerical tests, a free-free beam with only one-rigid-body mode in translation and a simply supported beam are used. For the experimental test, a free-free aluminum beam is utilized.

4.1 Numerical evaluation 1: free-free beam

4.1.1 Test model for numerical evaluation

A 1-D free-free beam with only one rigid-body mode in translation was assumed for numerical evaluation of the proposed modal identification approach. Note that the free-free beam has two rigid-body modes (translation and rotation). If signals from several sensors on the beam are measured, the signals would be the same and a mode-shape of the beam would be horizontally straight. The test configuration of the beam is shown in Fig. 3(a). Dynamic displacement from the j^{th} sensor on the i^{th} test beam, y_{ij} ($i = 1,2,..., m$; $j = 1,2,..., n$), was considered to a sine wave with damping as

$$y_{ij} = 0.03\sin(2\pi f_i t)e^{(-2\zeta_i \pi f_i t)} \tag{7}$$

where f_i and ζ_i are natural frequency and damping ratio, respectively, for rigid-body motion of the i^{th} test beam.

Three test beams with different natural frequencies ($m = 3$) were considered in this study as 10 Hz, 20 Hz and 50 Hz. Note that the practically measurable modal frequency in large civil structures is generally less than 50 Hz. The damping ratio was fixed to 2% for each test beam. The number of sensors was considered to be 21 ($n = 21$). The 5,000 signal data with sampling rate of 500 Hz were calculated for each test beam by using MATLAB because the signal were fully decayed before 10 seconds. Modal values extracted for each test beam are constant at all sensor locations. Also, normalized modal values by a modal value at Sensor 1 (i.e., reference sensor) have unity as shown in Fig. 3(b).

4.1.2 Time-unsynchronization effect on modal identification

To evaluate the effect of time-unsynchronization on modal identification, the time-delay was artificially injected to each of 21 sensors. As outlined in Table 1, time-delay scenarios were designed

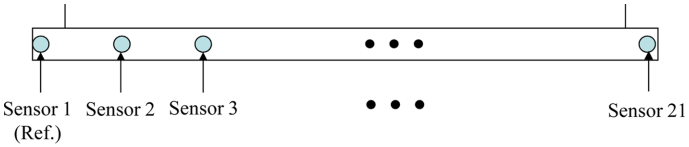

$$y_{ij} = 0.03\sin(2\pi f_i t)e^{(-2\zeta_i \pi f_i t)} \begin{cases} j = 1, 2, ..., 21 \\ \{f_{i=1,2,3}\} = \{10, 20, 50\} \\ \zeta_{i=1,2,3} = 2\% \end{cases}$$

(a) Structure and Test Configuration

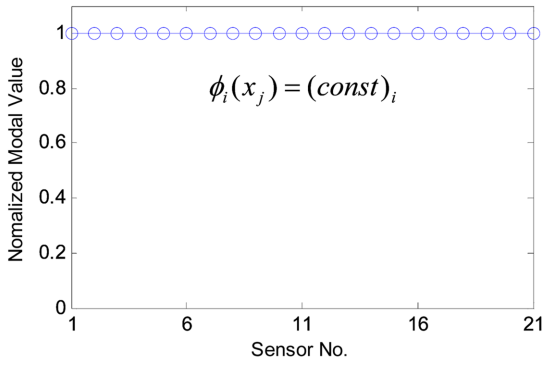

(b) Mode-Shape

Fig. 3 Free-free beam with a rigid-body motion and test configuration

Table 1 Time-delay scenarios for 21 sensors (Maximum of 50 ms delay)

Sensor No.	1	2	3	4	5	6	7
Delay (ms)	0	2.5	5	7.5	10	12.5	15
Sensor No.	8	9	10	11	12	13	14
Delay (ms)	17.5	20	22.5	25	27.5	30	32.5
Sensor No.	15	16	17	18	19	20	21
Delay (ms)	35	37.5	40	42.5	45	47.5	50

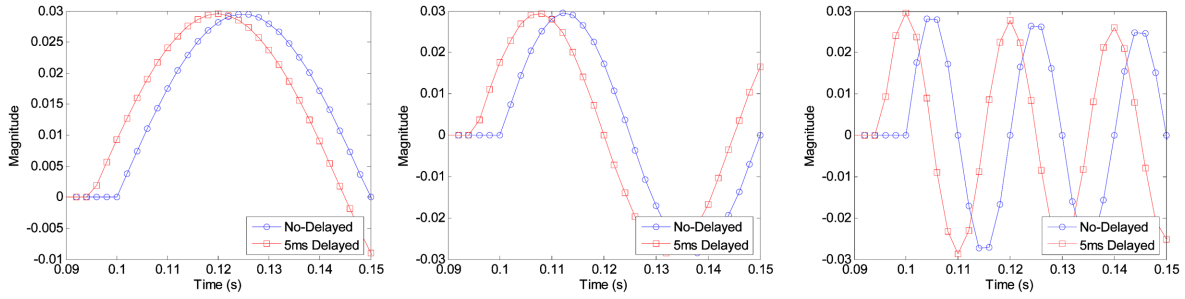

(a) Test Beam 1 (f=10 Hz) (b) Test Beam 2 (f=20 Hz) (c) Test Beam 3 (f=50 Hz)

Fig. 4 No-delayed original signals (Sensor 1) vs time-delayed signals (Sensor 3)

for 21 sensors. Given no-delayed Sensor 1 as the reference, the minimum time delay of 2.5 ms was set to Sensor 2 and the maximum time delay of 50 ms was set to Sensor 21. Fig. 4 shows no-

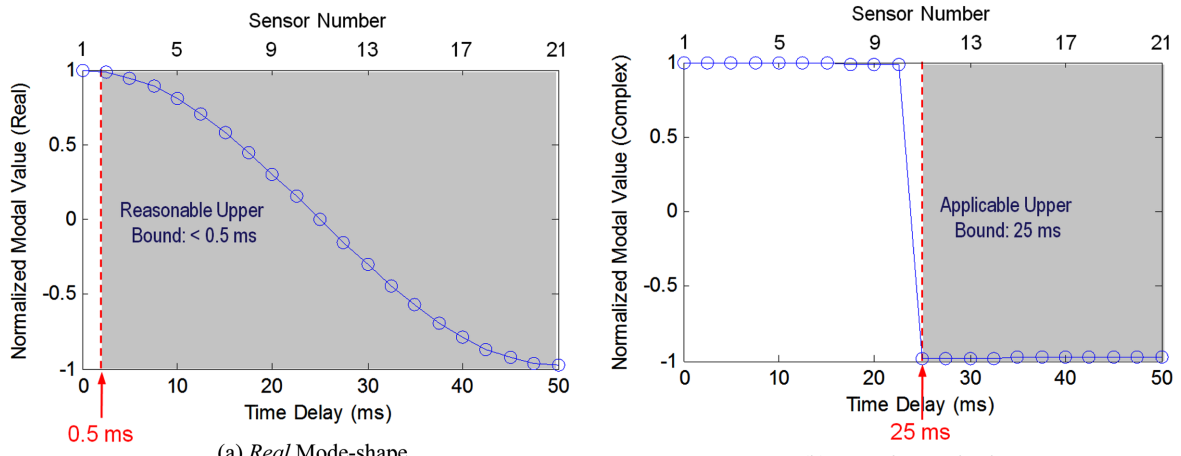

(a) *Real* Mode-shape (b) *Complex* Mode-shape

Fig. 5 Mode shapes of test beam 1 (f = 10 Hz) for maximum delay of 50 ms

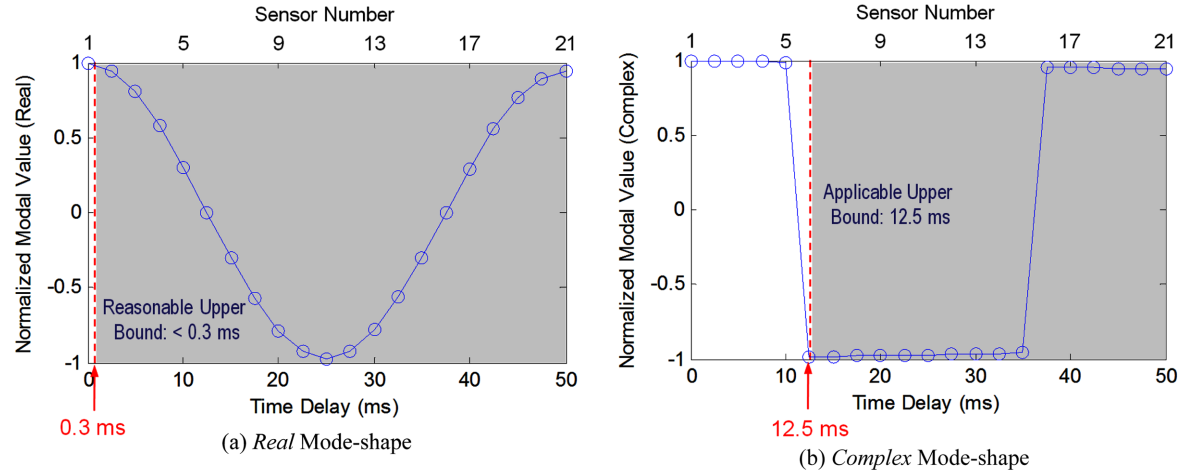

(a) *Real* Mode-shape (b) *Complex* Mode-shape

Fig. 6 Mode shapes of test beam 2 (f = 20 Hz) for maximum delay of 50 ms

delayed original signals from Sensor 1 and 5 ms-delayed signals from Sensor 3 for 10 Hz (Test Beam 1), 20 Hz (Test Beam 2), and 50 Hz (Test Beam 3), respectively.

For FFT process, 4,096 signal data obtained from each sensor were applied to the FDD method. Also, a rectangular window was applied but without using the overlapping technique. The FDD results for the three test beams are shown in Figs. 5-7. In the figures, the time-delays on the horizontal axis (0~50 ms) are corresponding to the sensor numbers (1~21, as listed in Table 1). Also, the normalized modal values, which were obtained using Sensor 1 (i.e., the no-delayed signals) as the reference, were measured with respect to each sensor that is matched to each time-delay.

In Fig. 5, the FDD results of Test Beam 1 with natural frequency of 10 Hz indicate: 1) time-delay induces error in *real* mode-shape after 0.5 ms and 2) *complex* mode-shapes are error-free if time-delay is less than 25 ms. In Fig. 6, the FDD results of Test Beam 2 with natural frequency of 20 Hz indicate: 1) time-delay induces error in *real* mode-shape after 0.3 ms and 2) *complex* mode-shapes

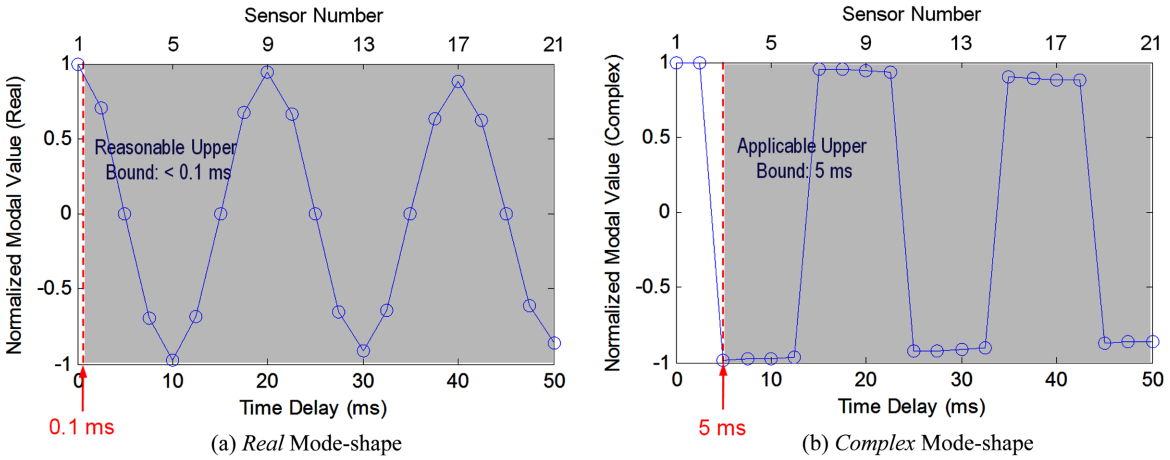

(a) *Real* Mode-shape (b) *Complex* Mode-shape

Fig. 7 Mode shapes of test beam 3 (f = 50 Hz) for maximum delay of 50 ms

are error-free if time-delay is less than 12.5 ms. In Fig. 7, the FDD results of Test Beam 3 with natural frequency of 50 Hz indicate: 1) time-delay induces error in *real* mode-shape after 0.1 ms and 2) *complex* mode-shapes are error-free if time-delay is less than 5 ms.

In the figures, *real* mode-shapes were completely affected by the time-delays. Modal values of the *real* mode-shapes were changed by any levels of time-delays. However, *complex* mode-shapes were not changed by the time-delays until the mode shape phases were changed larger than 90 degree. Note that the sign of the *complex* mode-shape in Eq. (5) is changed when the mode-shape phase is larger than 90 degree. From these results, an upper limit of time-delay for the proposed approach using the *complex* mode-shape is decided as follow

$$t_0^{Lim} < \frac{1}{4f_{Target}} \tag{8}$$

where t_0^{Lim} is the upper limit of time-delay for using the *complex* mode-shape and f_{Target} is the highest natural frequency considered for modal identification.

In general, time-delay occurred in wireless sensor nodes is less than a few milliseconds when a time-synchronization algorithm is adopted in wireless sensor network (Mechitov *et al.* 2004, Elson *et al.* 2002, Maroti *et al*. 2004). Therefore, additional tests were performed for the maximum time-delay of 2 ms as shown in Table 2. In Figs. 8-10, the time-delays on the horizontal axis (0-2 ms) are corresponding to the sensor numbers (1~21, as listed in Table 2). Also, the vertical axis represents normalized modal values with respect to Sensor 1 (i.e., the no-delayed signals). In Figs. 8-10, the

Table 2 Time-delay scenarios for 21 sensors (Maximum of 2 ms)

Sensor No.	1	2	3	4	5	6	7
Delay (ms)	0	0.1	0.2	0.3	0.4	0.5	0.6
Sensor No.	8	9	10	11	12	13	14
Delay (ms)	0.7	0.8	0.9	1.0	1.1	1.2	1.3
Sensor No.	15	16	17	18	19	20	21
Delay (ms)	1.4	1.5	1.6	1.7	1.8	1.9	2.0

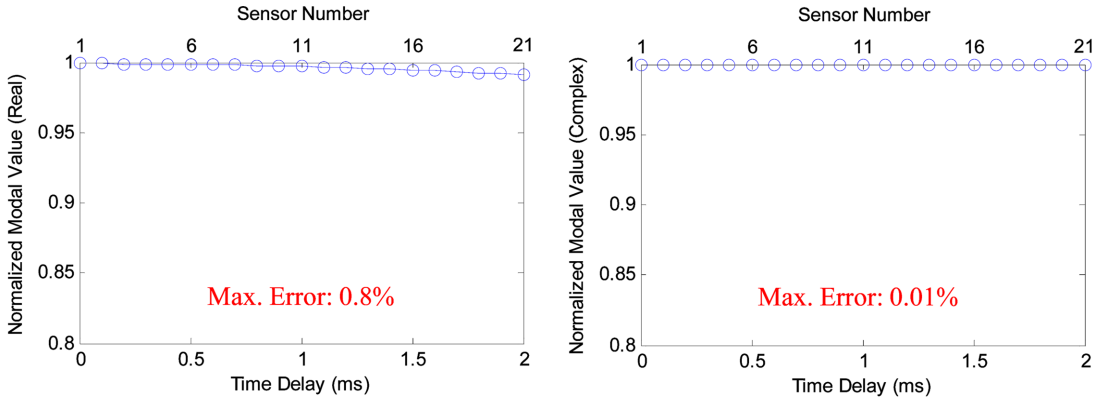

(a) *Real* Mode-shape (b) *Complex* Mode-shape

Fig. 8 Mode Shapes of Test Beam 1 (f = 10 Hz) for maximum delay of 2 ms

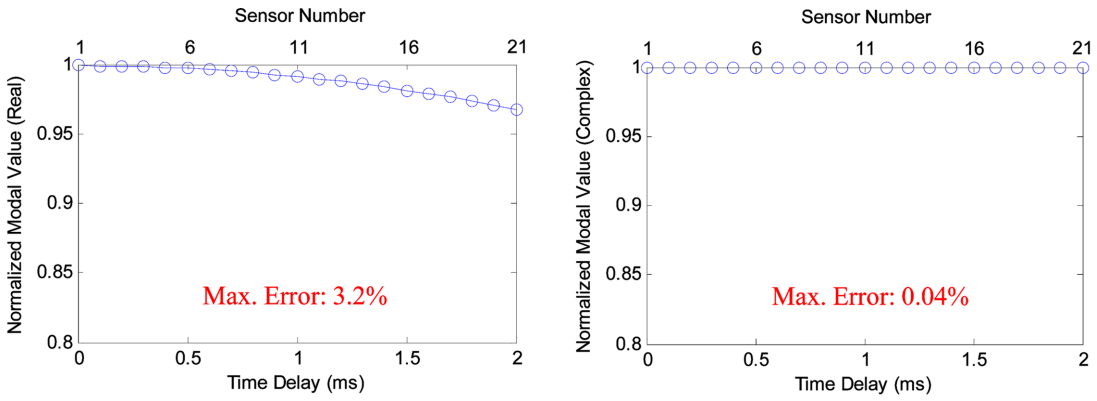

(a) *Real* Mode-shape (b) *Complex* Mode-shape

Fig. 9 Mode shapes of test beam 2 (f = 20 Hz) for maximum delay of 2 ms

maximum time-delay of 2 ms induces the maximum errors in *real* mode-shapes as follows: 0.8% for Test Beam 1 (f = 10 Hz), 3.2% for Test Beam 2 (f = 20 Hz), and 19.2% for Test Beam 3 (f = 50 Hz), respectively. Meanwhile, *complex* mode-shapes remain almost error-free with the maximum errors of 0.01%, 0.04% and 0.08%, respectively. Note that those errors are negligibly small in practice.

To evaluate the performance of the proposed output-only modal identification approach, random time-delay within 2 ms was injected for each sensor. Fig. 11(a) shows the time-delays applied for 21 sensors. The maximum time delay is about 1.8 ms at Sensor 17 and the minimum time-delay is about 0.002 ms at Sensor 18. Figs. 11(b)-11(d) show *real* mode-shapes and *complex* mode-shapes identified for the three test beams. For each test beam, the maximum error of *real* mode-shape due to the time-delay is appeared at Sensor 17 which has the maximum time-delay. Meanwhile, the complex mode-shapes remain almost error-free with the maximum errors of 0.003%, 0.001% and 0.01%, respectively. These results are similar to those of Figs. 8-10. However, the minimum errors of both *real* and *complex* mode-shapes were occurred at Sensor 15 since the mode-shapes calculated by the FDD method were normalized. Note that the minimum time-delay was injected at Sensor 18.

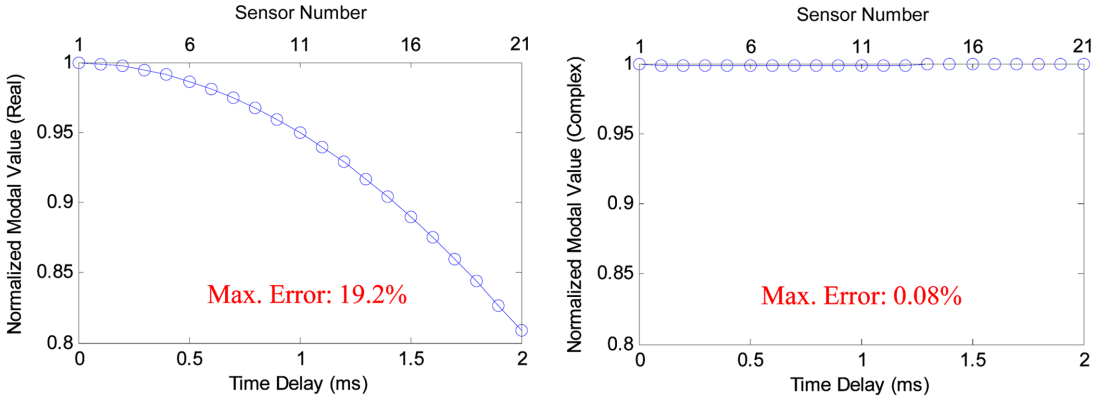

(a) *Real* Mode-shape (b) *Complex* Mode-shape

Fig. 10 Mode shapes of test beam 3 (f = 50 Hz) for maximum delay of 2 ms

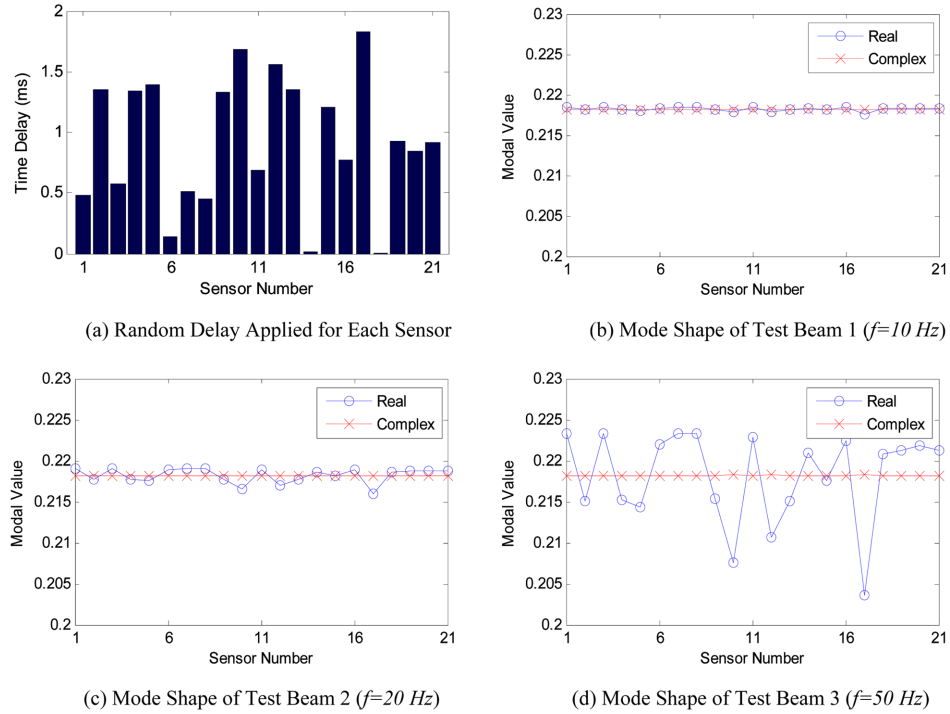

(a) Random Delay Applied for Each Sensor (b) Mode Shape of Test Beam 1 (*f=10 Hz*)

(c) Mode Shape of Test Beam 2 (*f=20 Hz*) (d) Mode Shape of Test Beam 3 (*f=50 Hz*)

Fig. 11 Mode shape of three test beams for random time-delay

4.1.3 Noise effect on modal identification

To evaluate the effect of noise on modal identification, white noises were injected in original signals. As shown in Table 3, the maximum noise level is about 20% in root-mean-square (RMS) level. For FFT process, 4,096 data obtained from each sensor were applied to the FDD method. Also, a rectangular window was applied but without using overlapping technique PSD calculation. The FDD results for the test beams are shown in Figs. 12(a)-12(c). In the figures, the noise level on the horizontal axis is corresponding to sensor numbers (see Table 3) and the vertical axis is modal values normalized by a modal value obtained from Sensor 1 (i.e., original signal). As shown in Fig.

Table 3 Injected-white noises for 21 sensors

Sensor No.	1	2	3	4	5	6	7
Noise (%)	0	1	2	3	4	5	6
Sensor No.	8	9	10	11	12	13	14
Noise (%)	7	8	9	10	11	12	13
Sensor No.	15	16	17	18	19	20	21
Noise (%)	14	15	16	17	18	19	20

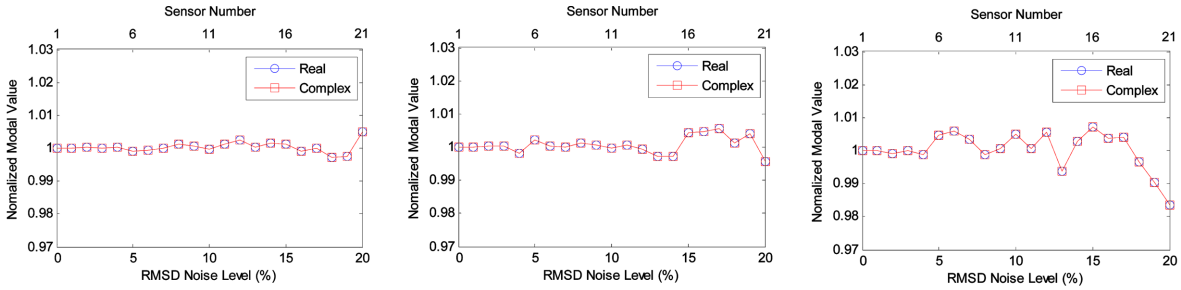

(a) Test Beam 1 (10 Hz) (b) Test Beam 2 (20 Hz) (c) Test Beam 3 (50 Hz)

Fig. 12 FDD results for signals with white noise: *Real* vs *Complex* mode-shapes

12, both of the *real* mode-shapes and *complex* mode-shapes are changed by noises. However, the relative differences between the two sets of mode-shapes are less than 0.02%. It is noticed that the change in the mode-shape phase caused by the injected noise is very small.

4.2 Numerical evaluation 2: simply supported beam

4.2.1 Test model for numerical evaluation

To evaluate the applicability of the proposed output-only modal identification approach, additional tests were numerically performed for a simply supported steel beam. The beam model with span length of 12 m was established by line elements as shown in Fig. 13. The material properties of the beam model are as follows: the elastic modulus $E = 200$ GPa, moment of inertia $I = 4.287\times10^{-5}$ m^4, mass density $m = 7{,}860$ kg/m^3 and Poisson's ratio $\upsilon = 0.3$.

To calculate acceleration responses of the test beam by impact force, the first three bending modes were considered in this study. The natural frequencies for the first three bending modes are 6.524 Hz, 25.907 Hz, and 57.463 Hz, respectively. The impact force was excited at a location of Sensor 3. Modal damping of 5% was applied for each mode. The 3,000 acceleration data with sampling rate of 1 kHz were acquired from the 9 sensor locations by using a finite element (FE) analysis software SAP2000. The acceleration signals were fully decayed before 3 seconds.

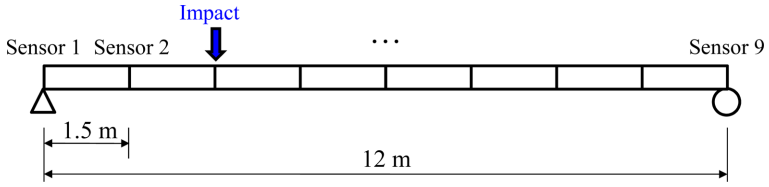

Fig. 13 Simply supported beam and test configuration

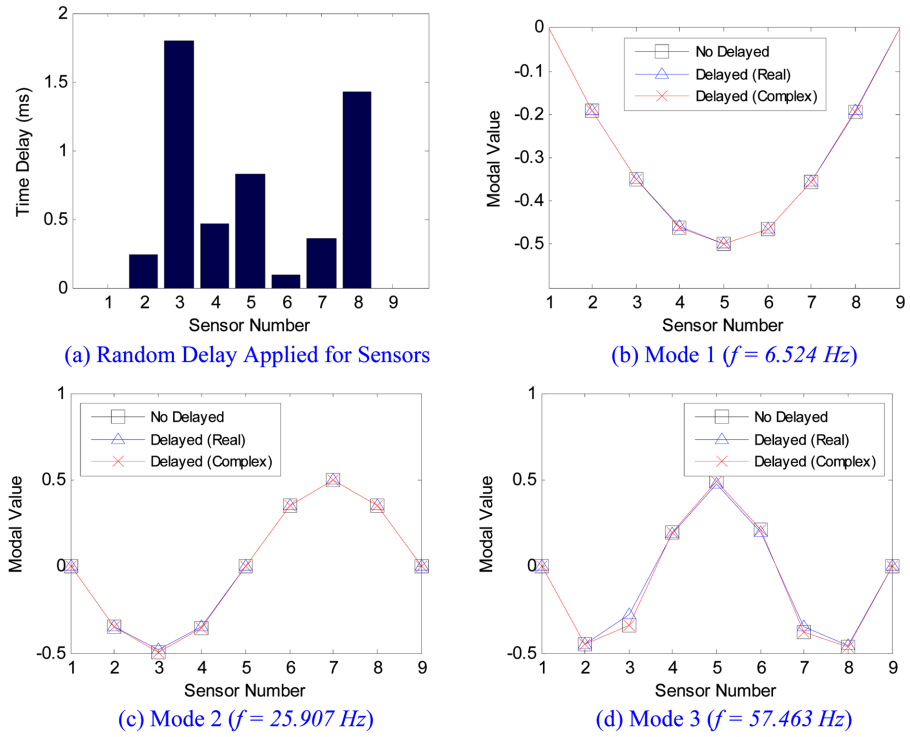

(a) Random Delay Applied for Sensors (b) Mode 1 ($f = 6.524$ Hz)

(c) Mode 2 ($f = 25.907$ Hz) (d) Mode 3 ($f = 57.463$ Hz)

Fig. 14 Mode shapes of simply supported beam for random delay

4.2.2 Time-unsynchronization effect on modal identification

To investigate the time-unsynchronization effect, random time-delay within 2 ms was artificially injected for Sensors 2-8. Note that the acceleration responses from Sensor 1 and Sensor 9 are unrelated to the time-synchronization since they have zero values. Fig. 14(a) shows the time-delays applied for the 7 sensors. The maximum time delay is about 1.8 ms at Sensor 3 and the minimum time-delay is about 0.09 ms at Sensor 6. Figs. 14(b)-14(d) show original mode-shapes extracted from acceleration signals without time-delay, and they are compared with time-delayed *real* mode-shapes and time-delayed *complex* mode-shapes extracted from acceleration signals with time-delay. The differences between the original mode shapes and time-delayed *real* and *complex* mode shapes

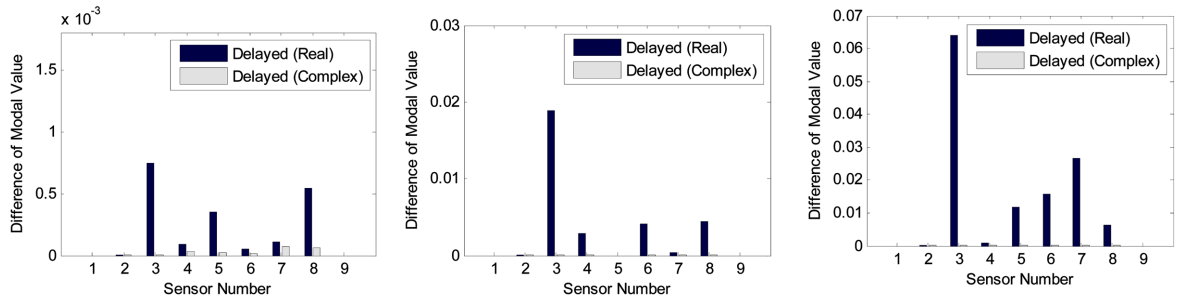

(a) Mode 1 (b) Mode 2 (c) Mode 3

Fig. 15 Mode shape differences due to time-delay for simply supported beam

were calculated as shown in Fig. 15. For each mode, the maximum difference of *real* mode-shape due to the time-delay is appeared at Sensor 3 which has the maximum time-delay. Meanwhile, the complex mode-shapes for the first three bending modes remain almost error-free with the maximum differences of 0.0684×10^{-3}, 0.0151×10^{-3} and 0.012×10^{-3}, respectively. These results are similar to those of the previous tests on the free-free beams.

4.3 Experimental evaluation

4.3.1 Test beam for experimental evaluation

As described in Fig. 16, a free-free aluminum beam was selected as a test structure. The geometrical and material properties of the test beam are as follows: the length $L = 0.56$ m, the rectangular cross-section $t \times H = 0.01$ m $\times$ 0.04 m, the elastic modulus $E = 70$ PGa, Poisson's ratio $\upsilon = 0.33$, and mass density 2700 kg/m^3.

The structural geometry and experimental layout with sensor arrangements are shown in Fig. 16(a). Seven accelerometers were selected to measure the motion of the structure in the z-direction (i.e., the vertical direction to sense out-of-plane motions) and equally distanced (i.e., 0.092 m) along the longitudinal direction. Impulse loads were applied to a location 0.06 m distanced from the left edge (e.g., about one-ninth of span length) by using a Dytran impulse hammer 5801A. Acceleration responses were measured by using Dytran 3101BG miniature accelerometers mounted along the center line. The accelerometers have the sensitivity of 10 mV/g, the measurable frequency range of 1 Hz - 10 kHz and the measurable acceleration range of -500 g - 500 g. A data acquisition system which included two 8-channel, 24-bit National Instrument PXI-4472 data acquisition (DAQ) cards, PXI-8186 controller, and LabVIEW was set up to measure signals from the accelerometers. Sampling frequency was set to 8.0 kHz and total 8,450 discrete data were acquired from each measure, by considering preliminary information on target frequency range of 0 - 2 kHz of the target structure.

Four damage scenarios were selected as listed in Table 4 and also depicted in Fig. 17. Two cracks were inflicted at a point near the center ($x/L = 0.466$) and another near the right edge ($x/L = 0.935$).

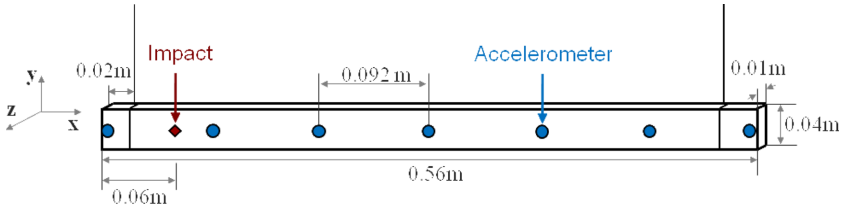

(a) Geometry of Free-Free Beam

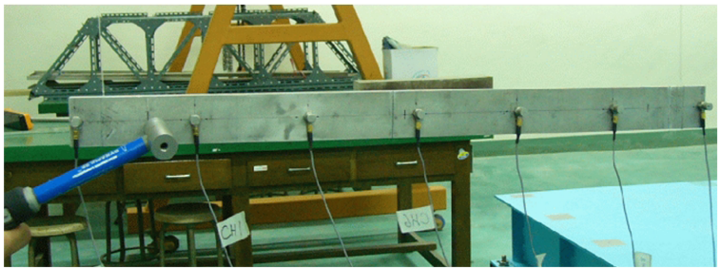

(b) Experimental Layout

Fig. 16 Experimental setup on free-free beam

Table 4 Damage scenario of experimental tests

Case	Damage location (x/L)	Damage size (a/t)
Damage 1	0.466	0.25
Damage 2	0.466	0.5
Damage 3	0.466, 0.935	0.5, 0.25
Damage 4	0.466, 0.935	0.5, 0.5

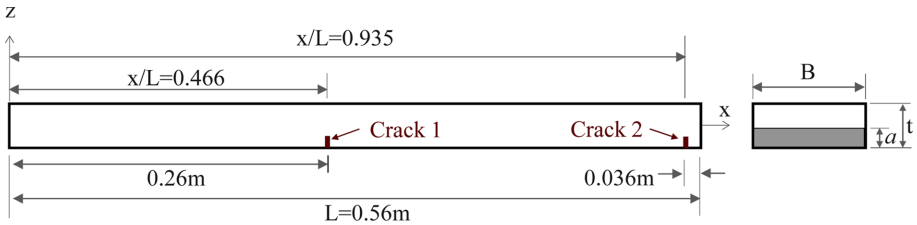

(a) Damage Locations

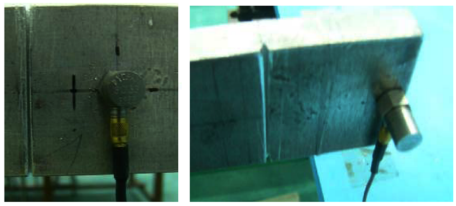

(b) Sawed Cuts (Crack 1 and Crack 2)

Fig. 17 Damage locations and sawed cuts

Also, two levels of damage-sizes were introduced by sawing off 25% ($a/t = 0.25$) and 50% ($x/L = 0.5$) of the beam thickness (t), respectively, as shown in Fig. 17(a).

4.3.2 Damage effect on modal identification

For the undamaged and 4 damage cases, experimental tests were performed to analyze the effect of damage on modal identification. *Real* mode-shapes (see Fig. 18) and *complex* mode-shapes (see Fig. 19) of the first four modes were extracted from the measured acceleration responses of the tests. The corresponding natural frequencies measured for the undamaged and 4 damage cases are outlined in Table 5. To investigate the effect of damage on modal identification, damage-induced changes in the *real* mode-shapes were compared with damage-induced changes in the *complex* mode-shapes of the four modes. Figs. 20 and 21 show the changes in the first four *real* and *complex* mode-shapes due to damage, respectively. That is, the "y" axis in Figs. 20-21 means the difference between modal values at the undamaged case and each damage case. The changes in mode shapes due to damage are almost identical, nonetheless of the choice of *real* or *complex* mode-shapes. Fig. 22 illustrates the differences between damage-induced changes in *real* mode shapes (i.e., Fig. 20) and those of *complex* mode-shapes (i.e., Fig. 21). For all of four modes, the changes are similar and negligibly small in practice.

4.3.3 Time-unsynchronization effect on modal identification

A set of data measured at undamaged state were used to investigate the effect of time-unsynchronization. As outlined in Table 6, time-delays of 0.125 ms and 0.25 ms were artificially

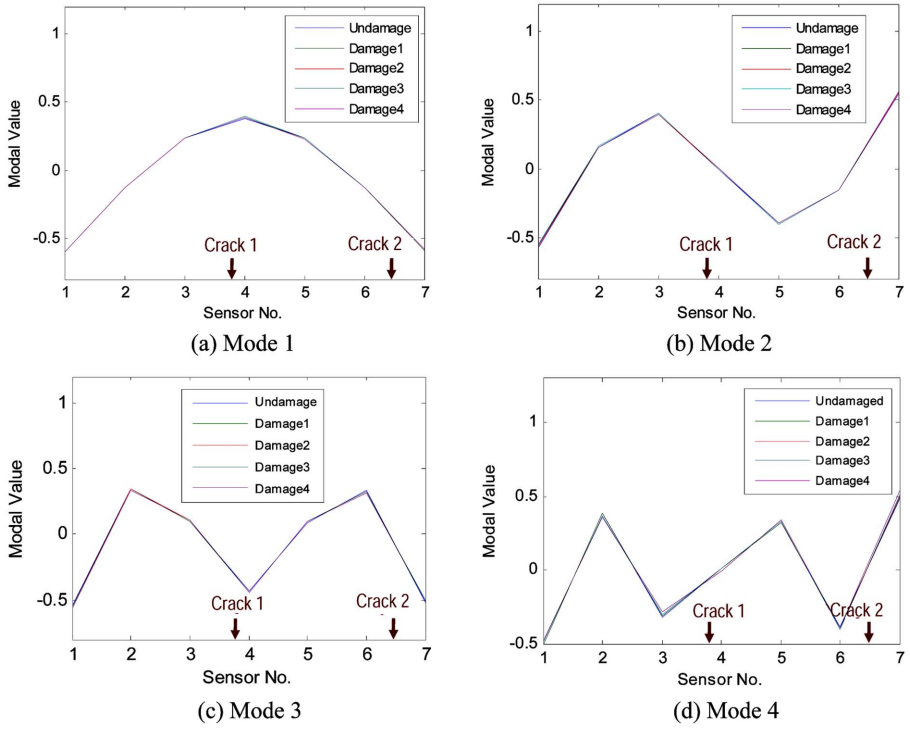

Fig. 18 *Real* mode-shapes measured for undamaged case and four damage cases

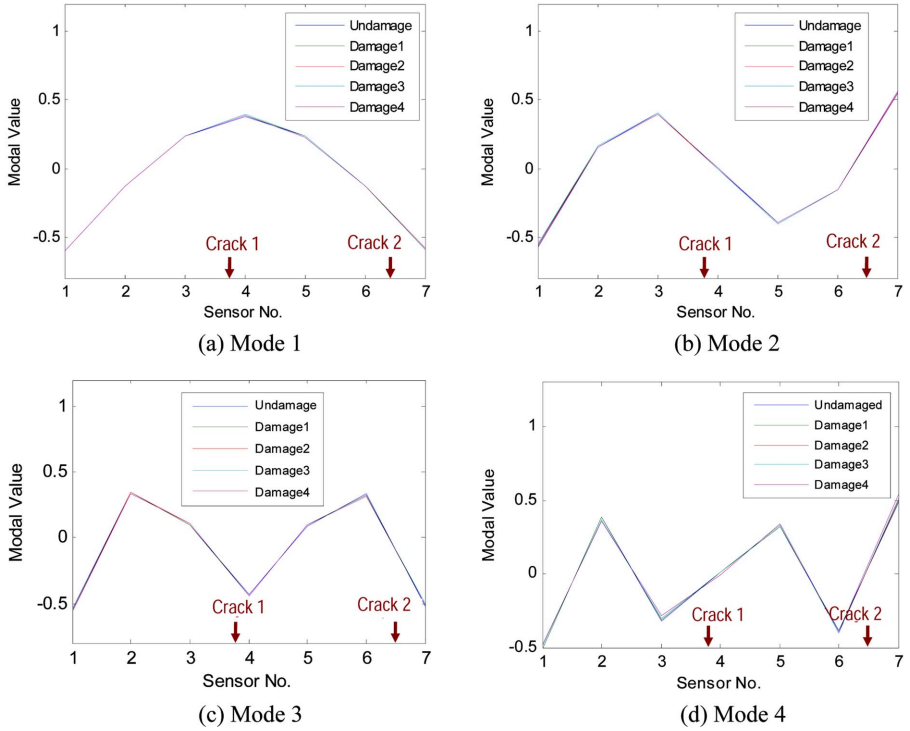

Fig. 19 *Complex* mode-shapes measured for undamaged case and four damage cases

Table 5 Natural frequencies for undamaged and four damage cases

Case	Natural frequency (Hz)			
	Mode 1	Mode 2	Mode 3	Mode 4
Undamaged	165.039	452.148	880.859	1445.31
Damage 1	163.086	451.172	873.047	1442.38
Damage 2	158.203	451.172	856.445	1436.53
Damage 3	158.203	450.195	855.469	1432.62
Damage 4	158.203	450.195	851.563	1416.02

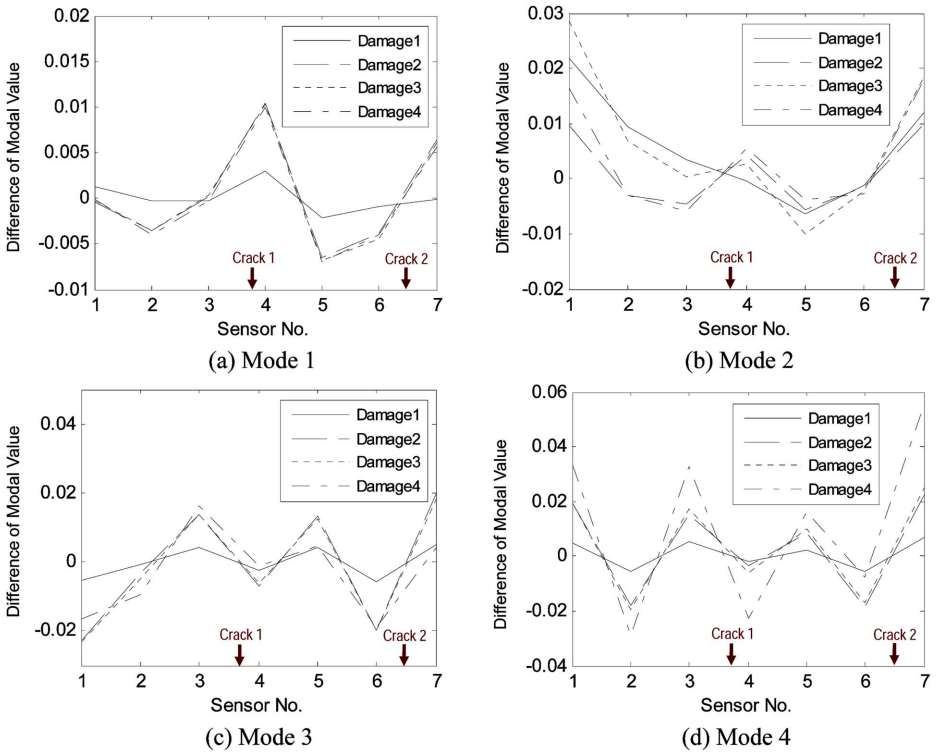

Fig. 20 Damage-induced *Real* mode-shape changes

injected into the acceleration data measured from Sensor 3, while the acceleration data of all other sensors remain on synchronized condition. That is, the normal signals of Sensor 3 were shifted into time-unsynchronized signals by time-delays of 0.125 ms and 0.25 ms, respectively. Note that results for the other sensors were similar to those for Sensor 3 since the proposed method is related to the time delays of a measurement system such as wireless sensors, but not structural vibration characteristics.

Next, the FDD method was utilized to extract *real* mode shapes and *complex* mode-shapes from the acceleration data of the seven sensors, among which Sensor 3 was unsynchronized as simulated in Table 6. Fig. 23 shows the first four *real* mode-shapes and Fig. 24 shows the corresponding *complex* mode-shapes. As shown in those figures, the *real* mode-shapes are changed remarkably in modes 2-4 due to both 0.125 ms and 0.25 ms time-delays but the *complex* mode-shapes remain

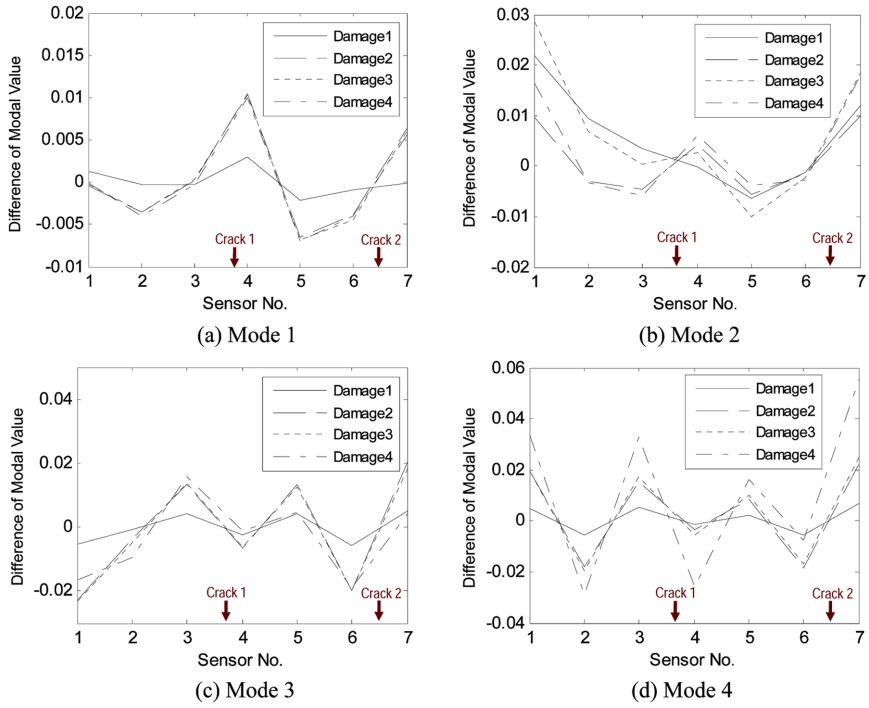

Fig. 21 Damage-induced *Complex* mode-shape changes

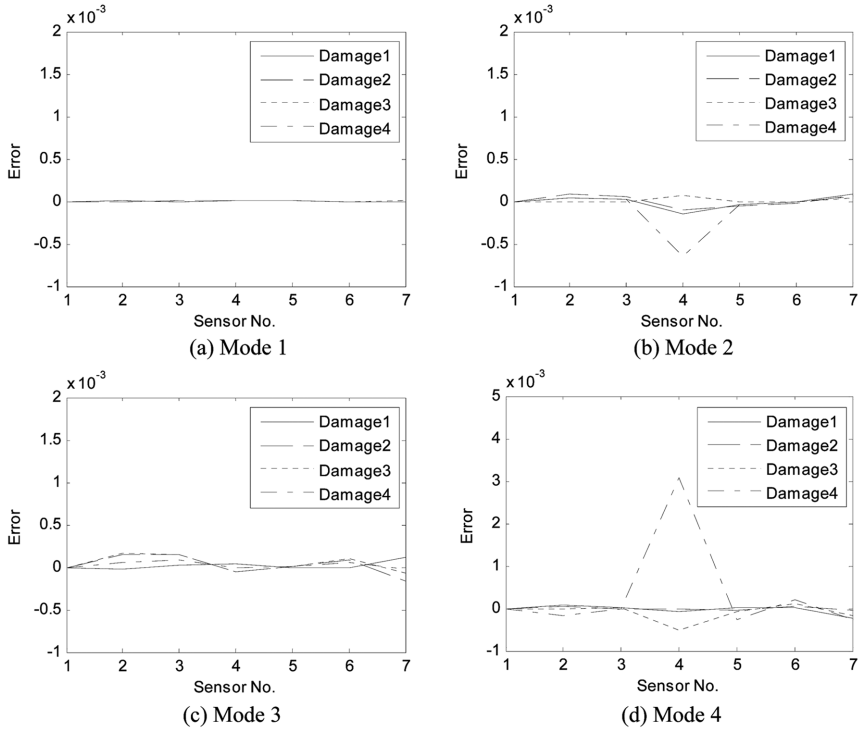

Fig. 22 Differences between damage-induced *Real* mode-shape changes and damage-induced *Complex* mode-shape changes

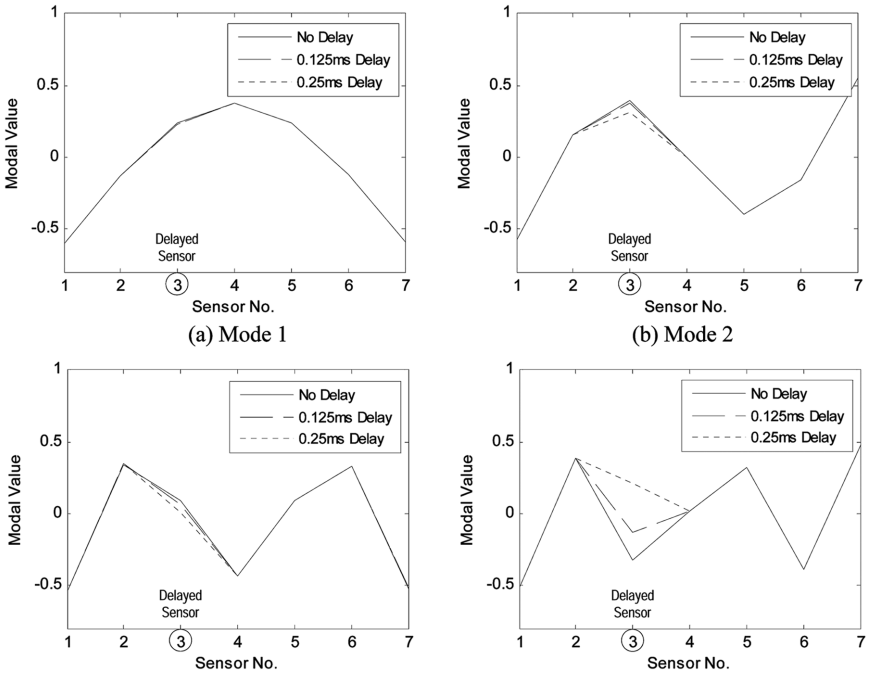

Fig. 23 *Real* mode-shape change due to time-delays

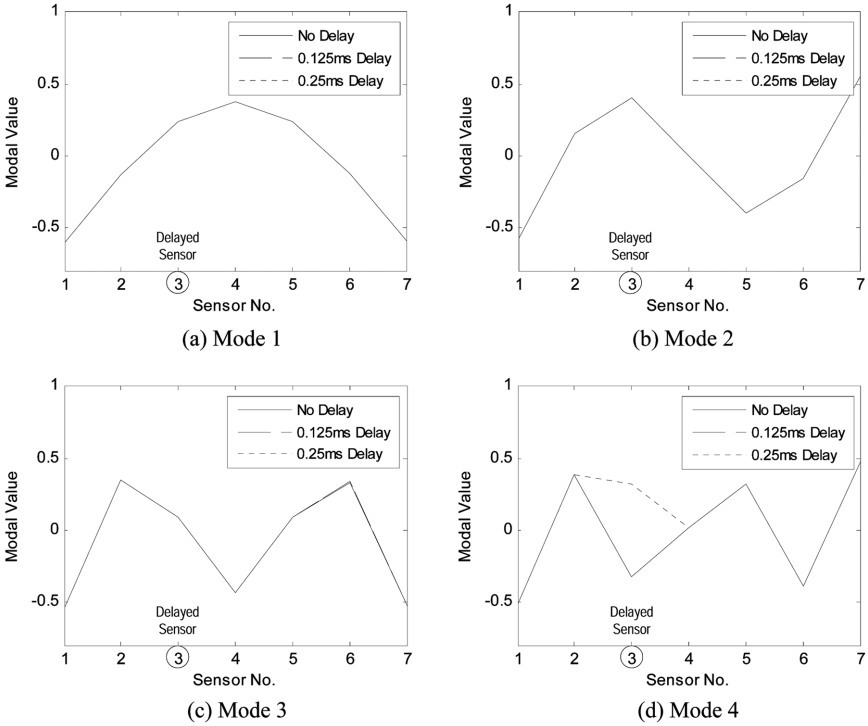

Fig. 24 *Complex* mode-shape changes due to time-delays

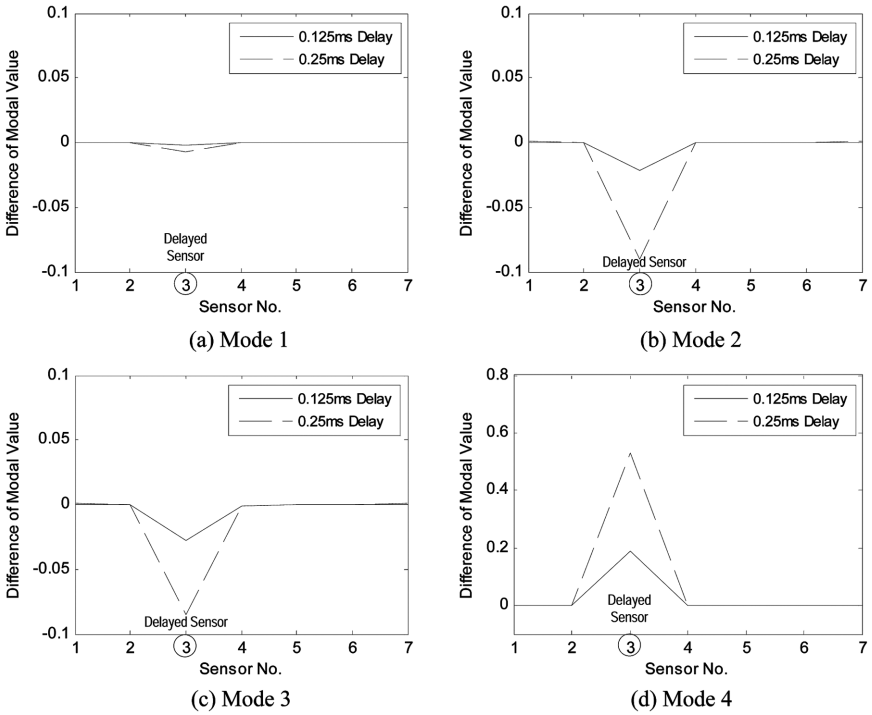

Fig. 25 Errors of *Real* mode-shapes due to time-delay

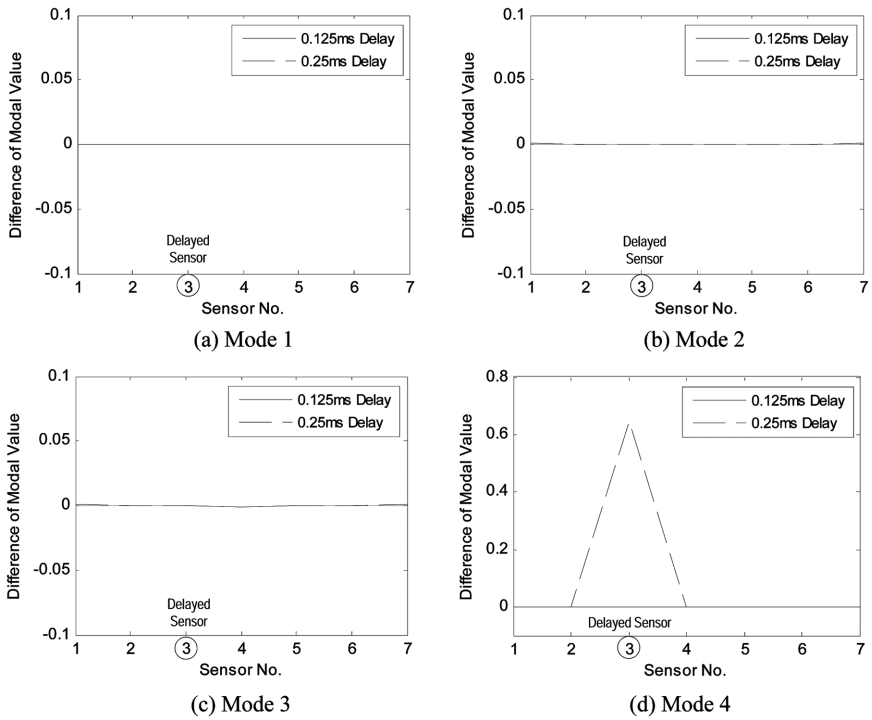

Fig. 26 Errors of *Complex* mode-shapes due to time-delay

Table 6 Artificially simulated time-delays in experimental data

Time-unchronized sensor	Time delay (ms)	
	Case 1	Case 2
Sensor 3	0.125	0.25

almost unchanged except in mode 4 (due to 0.25 ms time-delay). It is noticed that time-delays affected to mode shapes depending on the level of natural frequencies. As a lower frequency mode, mode 1 was less affected by the selected time-delays. But the other modes were relatively affected by the time-delays. In detail, the differences between the no-delayed and time-delayed results were calculated as shown in Figs. 25 and 26. As shown in Fig. 25, the time-delays lead to larger errors in higher modes of the *real* mode-shapes. As shown in Fig. 26, for the complex mode-shapes except mode 4 due to 0.25 ms time-delay, small errors are also occurred but the errors may be negligible in practice. Note that 0.25 ms time-delay for mode 4 exceeds the upper limit of time-delay for using the *complex* mode-shape (i.e., 0.173 ms estimated by Eq.(8)).

4.3.4 Time-unsynchronization effect on damage-induced mode shape changes

The unsynchronized data in Figs. 23 and 24 were further analyzed to investigate the effect of time-unsynchronization on damage-induced mode-shape changes. Note that the data measured from Sensor 3 was artificially simulated to generate unsynchronized time-delayed signals, as outlined in Table 6. The differences between *real* and *complex* modal values were calculated for the undamaged

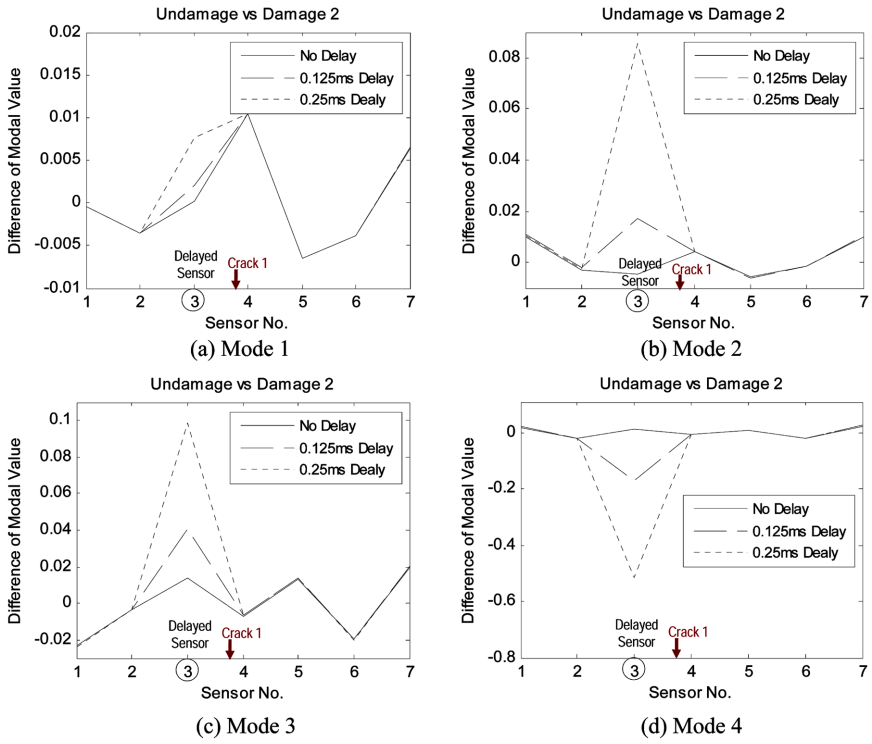

Fig. 27 Time-unsynchronization effect on damage-induced *Real* mode shape changes

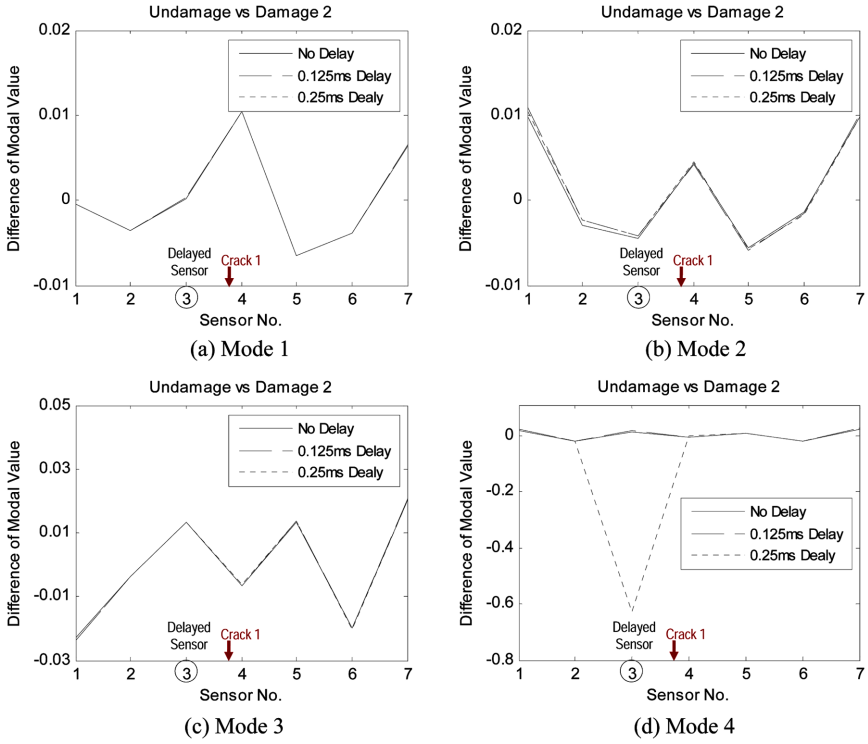

Fig. 28 Time-unsynchronization effect on damage-induced *Complex* mode shape changes

and four damage cases. The data measured at Damage Case 2 was used to investigate the effect of time-unsynchronization on damage-induced mode-shape changes. Note that one of the four damage cases (i.e., Damage Case 2) was presented since the results for the other damage cases were similar.

The effect of time-unsynchronization on damage-induced mode shape changes were estimated for *real* mode-shapes and *complex* mode-shapes, as shown in Figs. 27 and 28, respectively. For the *real* mode-shapes (Fig. 27), the time-delays lead to significant errors in damage-induced *real* mode-shape changes. These errors may result in false-alarms in mode-shape-based damage detection results. For the complex mode-shapes (Fig. 28), the time-delays cause relatively small errors except mode 4 due to 0.25 ms time-delay. Therefore, the feasibility of a mode shape measured by wireless sensors should be evaluated with respect to the allowable time-delay and the accuracy of damage-induced mode shape changes.

5. Conclusions

In this study, an output-only modal identification approach was proposed for decentralized wireless sensor nodes used for linear structural systems. The following approaches were implemented to achieve the objective. Firstly, an output-only modal identification method was selected for decentralized wireless sensor networks. Secondly, the effect of time-unsynchronization was assessed with respect to the accuracy of modal identification analysis. Time-unsynchronized signals were analytically examined to quantify uncertainties and their corresponding errors in modal identification results.

Thirdly, a modified approach using complex mode shapes was proposed to reduce the unsynchronization-induced errors in modal identification. In the new way, complex mode shapes were extracted from unsynchronized signals to deal both with modal amplitudes and with phase angles. Finally, the proposed approach was evaluated by numerical tests and experimental tests. From the evaluation, the following conclusions have been obtained:

(1) *Real* mode-shapes extracted from time-delayed signals included large errors in high frequency mode-shape; however, *complex* mode-shapes were almost error-free under the allowable time-delay;

(2) Both of the *real* mode-shapes and *complex* mode-shapes were changed by noises, but the relative differences between the two mode-shapes sets were very small. The change in the mode-shape phase caused by the injected noise was very small and negligible in practice;

(3) Damage-induced changes in mode shapes were almost identical, nonetheless of the choice of *real* or *complex* mode-shapes. Also, the differences between damage-induced changes in two mode-shapes sets were negligibly small; and

(4) For the *real* mode-shapes, the time-delays lead to significant errors in damage-induced *real* mode-shape changes. These errors may result in false-alarms in mode-shape-based damage detection results. For the complex mode-shapes, the time-delays cause relatively small errors except cases which exceed the upper limit of time-delay.

Acknowledgments

This study was financially supported by Pukyong National University in the 2010 Post-Doc. Program, National Research Foundation of Korea (NRF) through Smart Infra-Structure Technology Center (SISTeC) in the program year of 2009 and the second Brain Korea 21 Project in 2009.

References

Bendat, J.S. and Piersol, A.G. (1993), *Engineering applications of correlation and spectral analysis*, Wiley-Interscience, New York, NY.

Brincker, R., Zhang, L. and Andersen, P. (2001), "Modal identification of output-only systems using frequency domain decomposition", *Smart Materials and Structures*, **10**(3), 441-445.

Ewins, D.J. (2000) *Modal testing: theory, practice and application, second edition*, Research Studies Press LTD., Hertfordshire, England.

Elson, J., Girod, L. and Estrin, D. (2002), "Fine-grained network time synchronization using reference broadcasts", *Proceedings of 5th Symposium on Operating Systems Design and Implementation,* Boston, December.

Doebling, S.W., Farrar, C.R. and Prime, M.B. (1998), "A summary review of vibration-based damage identification methods", *Shock and Vibration Digest*, **30**(2), 91-105.

Farrar, C.R. (2001), *Historical overview of structural health monitoring, lecture notes on structural health monitoring using statistical pattern recognition*, Los Alamos Dynamics, Los Alamos, NM.

Hermans, L. and Van Der Auweraer, H. (1999), "Modal testing and analysis of structures under operational conditions: industrial applications", *Mechanical Systems and Signal Processing*, **13**(2), 193-216.

Ibrahim, S.R. and Mikulcik, E.C. (1977), "A method for the direct identification of vibration parameters from the free response", *Shock and Vibration Bulletin*, **47**(4), 183-198.

Juang, J.N. and Pappa, R.S. (1985), "An eigensystem realization algorithm for modal parameter identification and model reduction", *Journal of Guidance*, **8**(5), 620-627.

Kim, J.T., Ryu, Y.S., Cho, H.M. and Stubbs, N. (2003), "Damage identification in beam-type structures: frequency-based method vs mode-shape-based method", *Engineering Structures*, **25**(1), pp. 57-67.

Krishnamurthy, V., Fowler, K. and Sazonov, E. (2008), "The effect of time synchronization of wireless sensors on the modal analysis of structures", *Smart Materials and Structures*, **17**(5), 1-13.
Kurata, N., Spencer, B. F., and Ruiz-Sandoval, M. (2005), "Risk monitoring of buildings with wireless sensor networks", *Structural Control and Health Monitoring*, **12**(3-4), 315-327.
Lee, J.J. and Yun, C.B. (2006), "Two-step approaches for effective bridge health monitoring", *Structural Engineering and Mechanics*, **23**(1), 75-95.
Lu, K.C., Loh, C.H., Yang, Y.S., Lynch, J.P. and Law, K.H. (2008), "Real-time structural damage detection using wireless sensing and monitoring system", *Smart Structures and Systems*, **4**(6), 759-777.
Lynch, J.P., Sundararajan, A., Law, K.H., Kiremidjian, A.S., Kenny, T. and Carryer, E. (2003), "Embedment of structural monitoring algorithms in a wireless sensing unit", *Structural Engineering and Mechanics*, **15**(3), 385-297.
Lynch, J.P., Wang, W., Loh, K.J., Yi, J.H. and Yun, C.B. (2006), "Performance monitoring of the Geumdang bridge using a dense network of high-resolution wireless sensors", *Smart Materials and Structures*, **15**(6), 1561-1575.
Maia, N.M.M. and Silva, J.M.M. (1997), *Theoretical and experimental modal analysis*, Research Studies Press LTD., Hertfordshire, England.
Maroti, M., Kusy, B., Simon, G. and Ledeczi, A. (2004), "The flooding time synchronization protocol", *Proceedings of 2nd International Conference On Embedded Networked Sensor Systems,* Baltimore, November.
Mechitov, K.A., Kim, W., Agha, G.A. and Nagayama, T. (2004), "High-frequency distributed sensing for structure monitoring", *Proceedings of 1st International Workshop on Networked Sensing Systems*, Tokyo, June.
Nagayama, T. (2007), *Structural health monitoring using smart sensors*, Ph.D Dissertation, University of Illinois at Urbana-Champaign, Illinois, IL.
Nagayama. T., Sim, S. H., Miyamori, Y. and Spencer, B. F. (2007), "Issues in structural health monitoring employing smart sensors", *Smart Structures and Systems*, **3**(3), 299-320.
Nagayama, T., Spencer, B.F., Mechitov, K.A. and Agha, G.A. (2009), "middleware services for structural health monitoring using smart sensors", *Smart Structures and Systems*, **5**(2), 119-137.
Overschee, V.P. and De Moor, B. (1996), *Subspace identification for linear systems: theory – implementation - applications*, Kluwer Academic Publisher, Dordrecht, Netherlands.
Park, J.H., Hong, D.S., Kim, J.T., Todd, M.D. and Mascarenas D.L. (2008), "Development of smart sensor for hybrid health monitoring on PSC girders", *Proceedings of SPIE – International Symposium on Smart Structures and Materials*, San Diego, March.
Park, J.H. (2009), *Development of autonomous smart sensor nodes for hybrid structural health monitoring of large structures*, Ph.D. Dissertation, Pukyong National University, Busan, Korea.
Park, J.H. and Kim, J.T. (2009), "Presterss-force monitoring using wireless impedance sensor node in PSC girder nridges", *Proceedings of CTCS – The First International Conference on Computational Technologies in Concrete Structures*, Jeju, May.
Park, J.H., Kim, J.T., Hong, D.S., Mascarenas, D. and Lynch, J.P. (2010), "Autonomous smart sensor nodes for global and local damage detection of prestressed concrete bridges based on accelerations and impedance measurements", *Smart Structures and Systems*, **6**(5-6), 711-730.
Spencer, B.F., Ruiz-Sandoval, M.E. and Kurata, N. (2004), "Smart sensing technology: opportunities and challenges", *Structural Control and Health Monitoring*, **11**(4), 349-368.
Straser, E.G. and Kiremidjian, A.S. (1998), *A modular, wireless damage monitoring system for structure, Technical Report 128*, John A. Blume Earthquake Engineering Center, Stanford University, Stanford, CA.
Weng, J.H, Loh, C.H., Lynch, J.P., Lu, K.C., Lin, P.Y. and Wang, Y. (2008), "Output-only modal identification of a cable-stayed bridge using wireless monitoring system", *Engineering Structures*, **30**(7), 1820-1830.
Yi, J.H. and Yun, C.B. (2004), "Comparative study on modal identification methods using output-only information", *Structural Engineering and Mechanics*, **17**(3-4), 445-466.
Yi, J.H. (2001), *Damage assessment of structural joints using structural identification techniques*, Ph.D. Dissertation, Korea Advanced Institute of Science and Technology, Daejeon, Korea.
Zimmerman, A.T., Shiraishi, M., Swartz, R.A. and Lynch, J.P. (2008), "Automated modal parameter estimation by parallel processing within wireless monitoring systems", *ASCE, Journal of Infrastructures Systems*, **14**(1), 102-113.

CC